SEISMO-ACOUSTIC WAVE PROPAGATION IN ICE IN THE BALTIC SEA

Sven Ivansson [1]
Per Morén [1]
Torbjörn Ståhlsten [1]

[1] FOI (Swedish Defence Research Agency), SE-16490 Stockholm, Sweden

Abstract

Sound propagation under ice in the Baltic is of interest for military as well as civilian purposes. Important questions are, for example, how sonar systems are affected by ice in shallow waters and how marine mammal life under ice is affected by ship traffic. Compared to the normal case with a pressure-release surface, the ice gives rise to different boundary conditions for the sound propagation in the water column. In particular, the compressional- and shear-wave sound speeds in the ice are important parameters. The present paper describes how these sound speeds were determined in connection with an actual under-ice sound propagation trial in the Baltic. Three three-component geophones were deployed in the ice at distances between 50 and 100 m from a source point, where a sledge hammer was used to excite waves in the ice. Horizontally polarized shear waves and quasi-longitudinal plate waves were observed, from which the desired sound speeds could be obtained. The wave arrivals are successfully modeled using a wavenumber integration method.

Contact author: Ivansson, S., FOI, SE-16490 Stockholm, SWEDEN, email: sveni@foi.se

Introduction

An sea trial was made by FOI (the Swedish Defence Research Agency) in April 2013 in the Bothnian Bay in the northern part of the Baltic to measure underwater sound propagation in the presence of an ice cover. The test site is shown in Fig. 1. Judging by a few drill-hole samples, the ice thickness varied between 0.6 and 0.7 m except at ridge and keel locations. The measurement results, with 10-20 kHz under-ice propagation over a range of 5 km, are reported in Sangfelt et al. (2013). A ray model, Rev3D, was amended and used to model the measured propagation loss. The amendments, to handle a rough lower ice surface with randomly located keels and ray tracing in the ice, are described in Ivansson et al. (2014).

The present paper, however, deals with a special seismo-acoustic trial that was set up to determine the sound speeds in the ice. These sound speeds are needed for the ray modeling of the underwater sound propagation. The seismo-acoustic measurements are made at

much lower frequencies than the acoustic propagation measurements in the water, but the sound speeds in the ice are probably not very sensitive to the frequency.

The plan of the paper is as follows. A description of the seismo-acoustic trial is given first, along with the measured data. A modeling method is described next, where a wavenumber integration method for underwater sound propagation is adapted to seismo-acoustic sound propagation with sources of different types. Comparison of measured and modeled data subsequently provides a determination of the desired sound speeds. After some discussion, the paper is finalized by formulating the main conclusions.
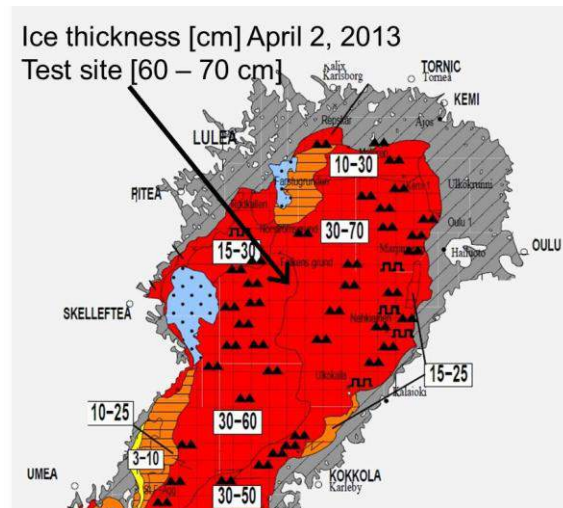

Figure 1: Test site in the Bothnian Bay.

Measurements

The set-up for the seismo-acoustic ice measurements is shown in Fig. 2. Measurements of this kind have previously been reported by Dosso et al. (2002). Three-component geophones were deployed on the ice along a line from a selected source point, where waves in the ice were generated by distinct sledge-hammer blows. A Cartesian coordinate system is introduced in Fig. 2, with horizontal x,y coordinates and a depth coordinate z. There are three geophone positions, at $x = 50.5$, 75, and 100 m on the x axis. Sledge-hammer blows were applied in all three coordinate directions: x, y, and z.
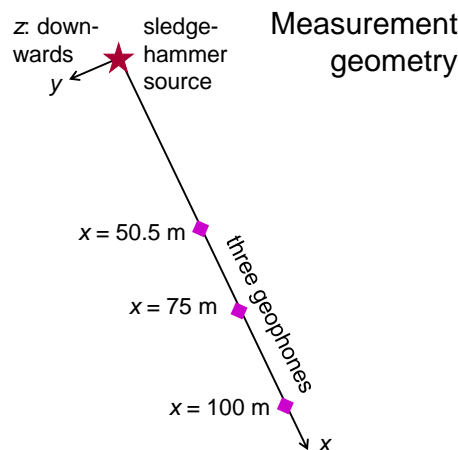

Figure 2: Measurement geometry in the horizontal x,y plane.

Figure 3 shows some recorded time traces. There is one panel for each of four source-receiver polarizations. Under ideal flat-ice conditions, well-known reciprocity results (Aki & Richards, 2002) predict that the $z{\rightarrow}x$ (for a vertical sledge-hammer blow and registrations of motion in the x direction) and $x{\rightarrow}z$ traces would be identical except for a sign change. This reciprocity does not show up, however, because the conditions are not ideal. Scattering from ice keels and ice ridges give rise to complex time signals.

Nevertheless, the $x{\rightarrow}z$ trace shows a clearly identifiable first arrival with move-out about 3200 m/s. A first arrival with this move-out can also been observed in the $x{\rightarrow}x$ trace.
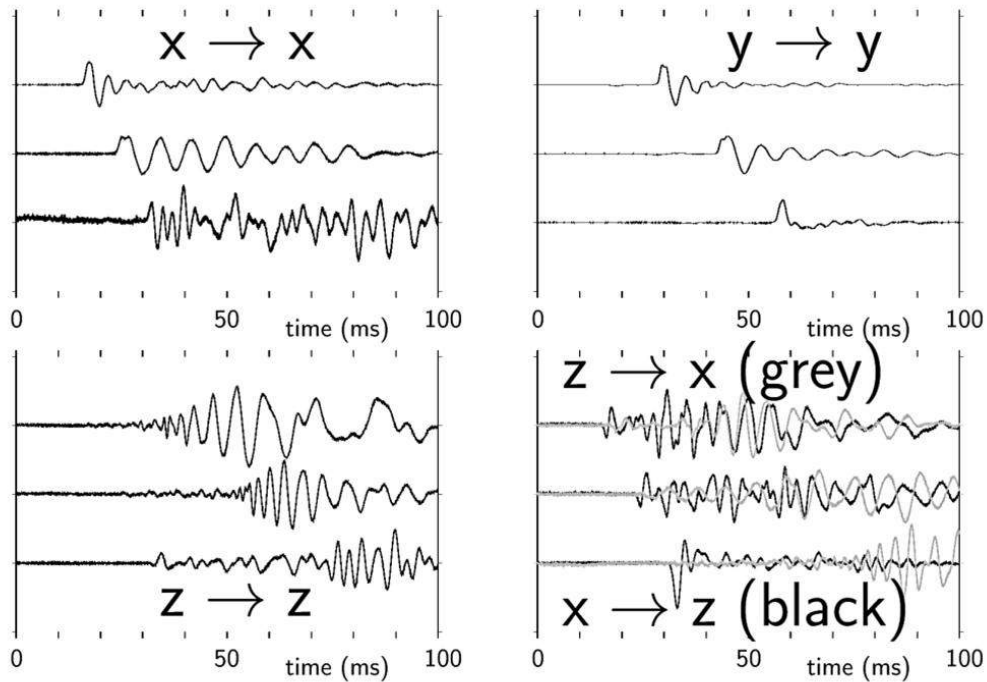

Figure 3: Measurement results, scaled to the same maximum amplitude for each time trace. There are four panels, one for each of four source-receiver polarizations. The notation z→x is used for a sledge-hammer blow in the z direction and a geophone recording in the x direction, etc. There are three time traces in each panel, from top to bottom in the order of increasing source-receiver separation.

The $y{\rightarrow}y$ panel has the simplest appearance, with virtually only one arrival. Its move-out is about 1800 m/s. In the two lower panels, for the $z{\rightarrow}z$, $x{\rightarrow}z$, $z{\rightarrow}x$ polarizations, there is a slow dispersive arrival, which is most clear in the $z{\rightarrow}z$ case.

From the literature, e.g., Ewing et al. (1957), one expects three kinds of wave arrivals under these circumstances: a horizontally polarized shear wave (SH) in the $y{\rightarrow}y$ case, a (quasi)longitudinal plate wave clearest visible in the $x{\rightarrow}x$ case, and a bending plate wave, the flexural wave, that is clearest visible in the $z{\rightarrow}z$, $x{\rightarrow}z$, $z{\rightarrow}x$ cases. Indeed, these three kinds of waves are observed in Fig. 3.

Under ideal flat-ice conditions, symmetry considerations show that a y source could not generate x or z registrations, and that an x or z source could not generate y displacements. In other words, P-SV and SH motions are decoupled (Aki & Richards, 2002), and the polarization pairs of interest are captured by Fig. 3.

Modeling

Figure 4 shows an idealized environmental model, with 0.65 m thick flat ice used for modeling the recorded time signals. Some ice data, that are actually not very important for the measured results in Fig. 3, are taken from the literature: density 900 kg/m^3, and absorption values of 0.4 and 1.0 dB/wavelength for compressional and shear waves, respectively. The measured sound speed profile in the water (not shown) is upward refracting, with an increase from 1405 m/s above the depth 43 m to 1422 m/s below the depth 58 m down to the bottom at a depth of 70 m. Below the bottom, there is a postglacial clay layer (thickness 5 m, sound speed 1450 m/s, density 1400 m/kg^3, absorption 0.2 dB/wavelength) above a half-space with glacial sand and fine grained moraine (sound speed 1550 m/s, density 1700 m/kg^3, absorption 0.2 dB/wavelength). The source and geophone positions are recognized from Fig. 2.
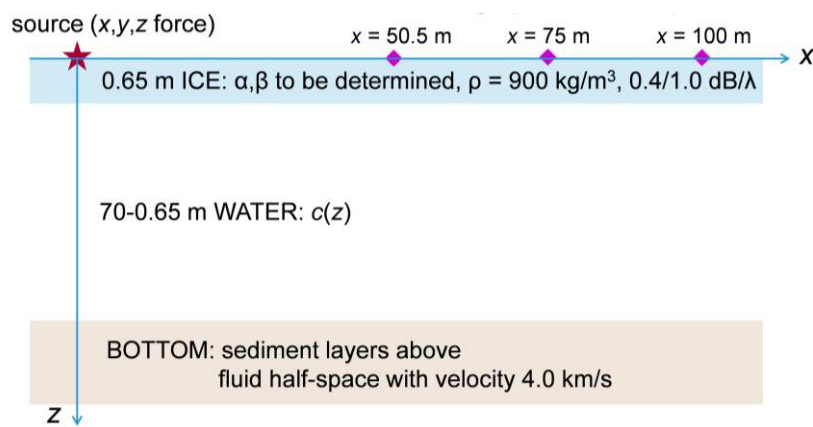

Figure 4: Environmental model used for wavenumber integration modeling. The compressional- and shear-wave sound speeds in the ice, denoted α and β, respectively, are to be determined.

The wavenumber integration code RPRESS (Ivansson, 1998) for seismo-acoustic wave propagation in laterally homogeneous fluid-solid media was amended to model the recorded time series. RPRESS combines a compound-matrix method (Ivansson, 1993 and 1997) for solving the pertinent ordinary differential-equation system in depth for each horizontal wavenumber k with an adaptive integration method (Ivansson and Karasalo, 1992) for the integration over k. The amendments concern, in particular, inclusion of dependence on azimuth (by a few Fourier-series terms) and implementation of equations for point-force excitation (Aki & Richards, 2002).

Comparison of measurements and modeling results

An initial problem in the modeling concerns selection of the source pulse, to mimic the sledge-hammer blows. The left panel of Fig. 5 shows a band-pass filtered Dirac pulse (upper trace) together with its first (middle trace) and second (lower trace) derivatives. An initial hypothesis was that the upper trace would be suitable for the body force. Since RPRESS produces particle displacement output, the time derivative (the middle trace) would be useful to model geophone registrations, which show particle velocities. The best match to the measured data was obtained by choosing the lower pulse, however.
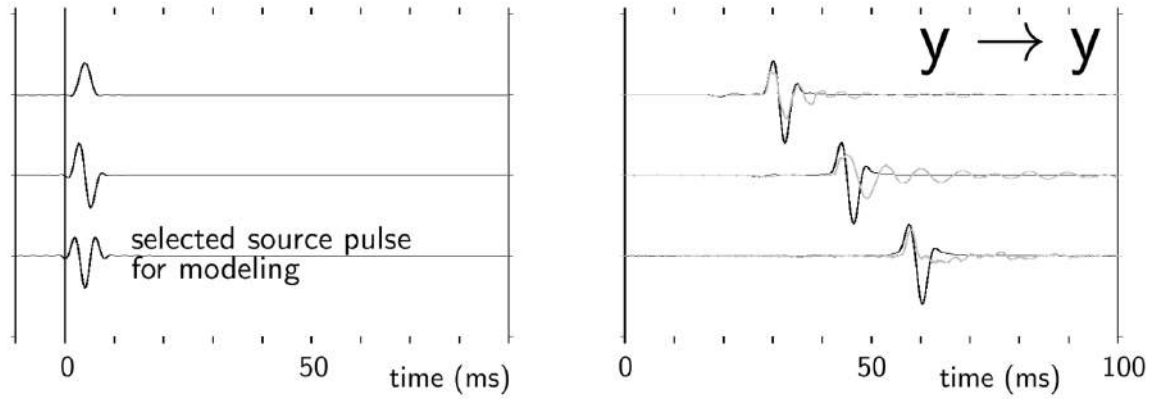
Figure 5: Left: selection of source pulse. Right: results for source and receiver in the y direction, grey/black is used for measured/modeled.

The right panel of Fig. 5 shows a comparison of measurements and modeling results for the SH wave, with the shear-wave sound speed β in the ice set to 1800 m/s for the modeling, as suggested by the move-out in the upper right panel of Fig. 3. As in Fig 3, as well as forthcoming figures, the traces are scaled to the same maximum amplitude. (The geophones were not accurately calibrated, implying that information on relative amplitudes among the traces is missing in the measured data.) The match between measured and modeled time traces is considered to be satisfactory, and the sound-speed estimate $\beta = 1800$ m/s is kept.

According to theory, e.g., Theorem 4.1 in Ivansson (1998), the low-frequency phase velocity of the quasi-longitudinal plate wave can be expressed as $2\beta(1- \beta^2/\alpha^2)^{1/2}$, where α and β are the compressional- and shear-wave sound speeds in the ice, respectively. Hence, the move-out 3200 m/s noted in the upper left panel of Fig. 3 suggests the estimate $\alpha = 3700$ m/s. A question is, of course, if the ice is sufficiently thin in relation to the wavelength to warrant applicability of the simple phase-velocity expression.
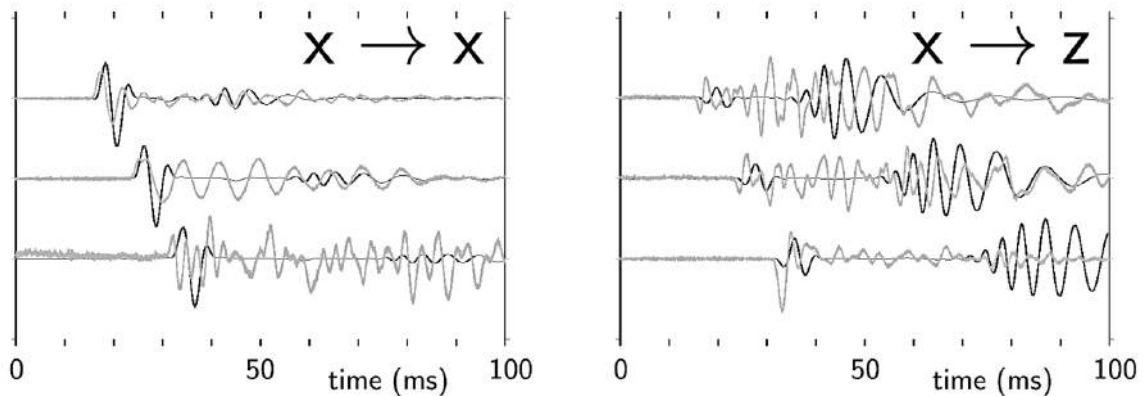

Figure 6: Results for source in the x direction, grey/black means measured/modeled. Left: receiver in the x direction. Right: receiver in the z direction.

With the mentioned sound speeds in the ice, Figs. 6 and 7 show comparisons of measured and modeled time traces of P-SV type. Indeed, the initial arrival is modeled reasonably well, particularly for the $x{\rightarrow}x$ polarization case in the left panel of Fig. 6. It is of course expected that the (quasi)longitudinal wave is best seen in this case. Because of its *quasi*-longitudinal nature, however, it can can also be observed in the $x{\rightarrow}z$ and $z{\rightarrow}x$ cases, cf. Theorem 4.4 and Eq. (4.13) in Ivansson (1998).

The dominant arrival in almost all the P-SV polarization cases of Figs. 6 and 7 is the dispersive bending plate wave. According to Theorem 6.1 in Ivansson (1998), its phase velocity (for a fluid bottom) decreases as $\omega^{3/5}$ when the angular frequency ω tends to zero, and the higher frequencies appear before the lower ones in the wave train. As expected, cf. Theorem 6.5 in Ivansson (1998), the bending wave is best seen in the $z \rightarrow z$ case.

A subtle detail that may be noted is that, for a solid bottom half-space in the modeling, the bending-wave phase velocity would decrease as $\omega^{2/3}$. The difference compared to the fluid-bottom modeling is only visible at extremely low frequencies, however, far beyond those considered in the present paper.
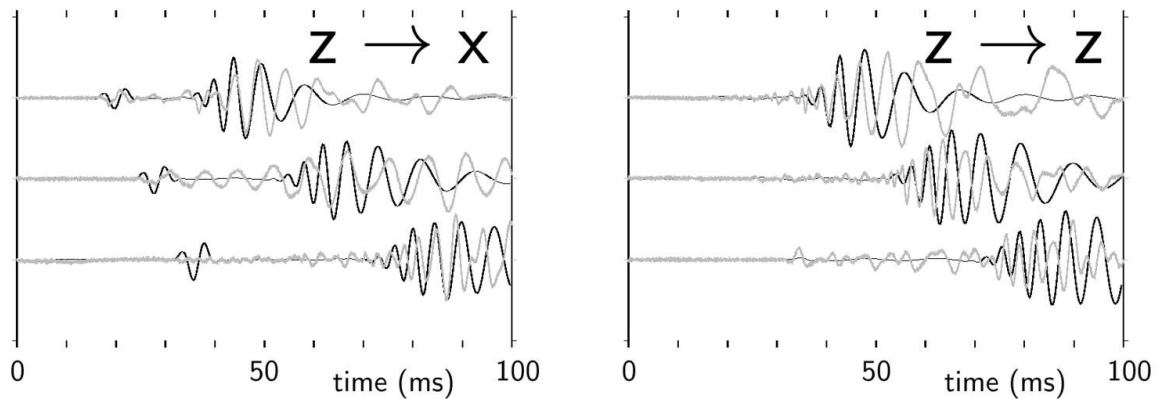

Figure 7: Results for source in the z direction, grey/black means measured/modeled. Left: receiver in the x direction. Right: receiver in the z direction.

Discussion

For a fluid bottom, Theorem 6.1 in Ivansson (1998) also shows that the low-frequency bending-wave phase velocity depends on the ice thickness h according to the factor $h^{2/5}$. As Fig. 7, Figs. 8 and 9 concern the $z \rightarrow x$ and $z \rightarrow z$ polarization cases, but the ice thickness is halved and doubled, respectively. As expected, the flexural wave appears later in Fig. 8 and earlier in Fig. 9. The match to the experimentally observed arrival is best in Fig. 7, however, indicating that 0.65 m is a reasonable value for the average ice thickness in the area.
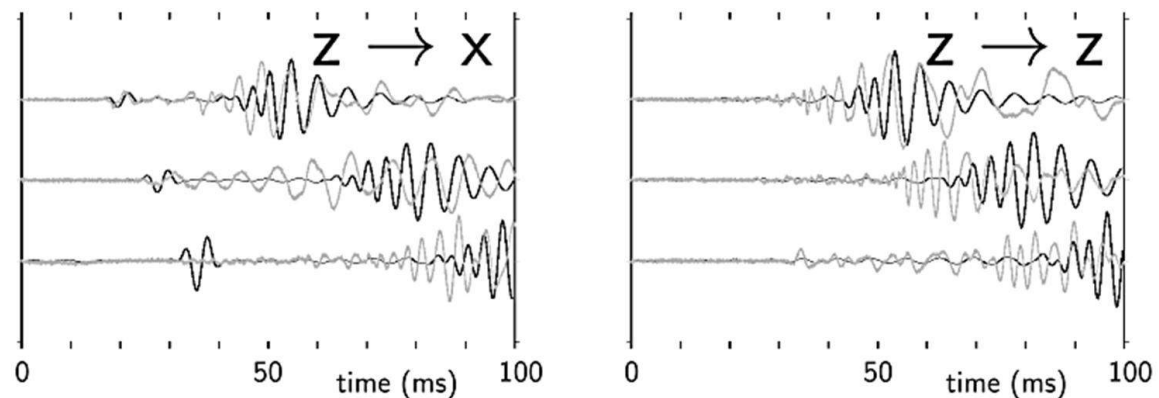

Figure 8: As Fig. 7 but with the modeling done for thin ice (0.325 m).

Stein et al. (1998) have suggested that the ice thickness could be determined by the quotient between the horizontal (x) and vertical (z) amplitudes of the flexural wave. As is also shown by Theorems 6.1, 6.5, and 6.6 in Ivansson (1998), the mentioned amplitude quotient multiplied with the flexural-wave phase velocity (and divided by the angular frequency ω) is proportional to the ice thickness h. In the present case, with a fluid bottom model, the amplitude quotient would be proportional to $h^{3/5}$. The applied scaling of the traces makes this effect somewhat difficult to observe in Figs. 7-9, however.
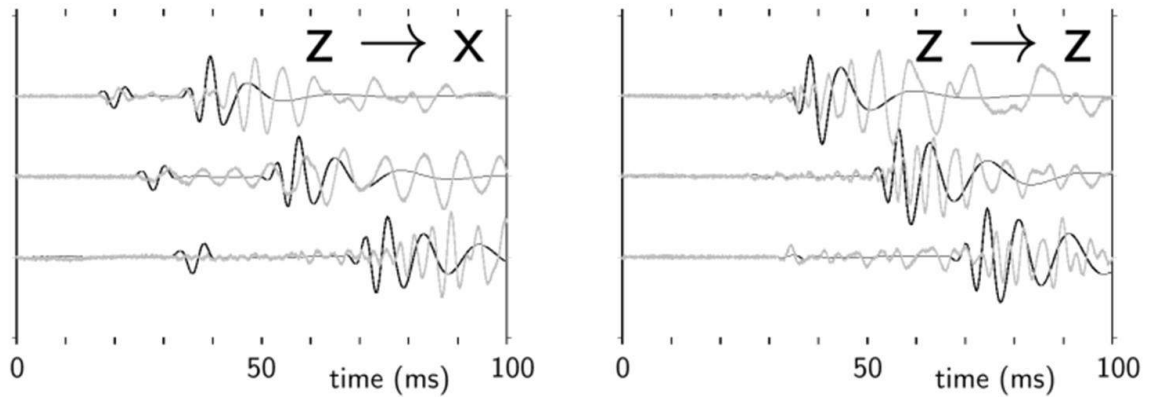

Figure 9: As Fig. 7 but with the modeling done for thick ice (1.3 m).

The $z{\to}x$ and $x{\to}z$ results from Fig. 3 are repeated in the right panel of Fig. 10. As already noted, scattering from ice keels and ice ridges destroy the reciprocity effect that would be observed under ideal conditions. (A reciprocity check in a laterally inhomogeneous environment would entail an actual physical change of source and receiver positions.) In the left panel, for the modeled time traces, the $z{\to}x$ and $x{\to}z$ traces are identical except for a sign change, however. This is a useful check of the computer code, since the computations are performed in rather different ways.
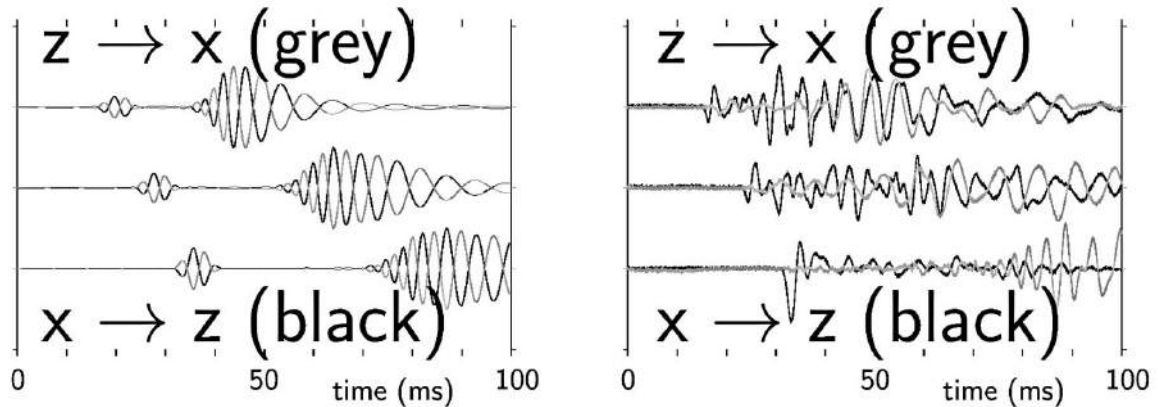

Figure 10: Reciprocity check for modeling (left) and measurements (right). The grey curves show $z{\to}x$ results (source in the z direction and receiver in the x direction), while the black curves show $x{\to}z$ results (source in the x direction and receiver in the z direction).

Conclusions

To support ray modeling of under-ice sound propagation in the Baltic, sound speeds in the ice have been determined by seismo-acoustic measurements and modeling. A sledge-

hammer source was used, with blows in different directions, to excite waves that were recorded with three three-component geophones. Three characteristic wave types showed up clearly in the recordings: a horizontally polarized shear wave (SH), a (quasi)longitudinal plate wave, and a dispersive flexural wave (bending plate wave).

A wavenumber integration code has been adapted to model the registered time traces. The SH wave recordings indicate an ice shear-wave sound speed of about 1800 m/s. Using the move-out of the quasi-longitudinal wave (about 3200 m/s), the compressional-wave sound speed in the ice is estimated to be about 3700 m/s. The modeling shows that the measured dispersion characteristics of the flexural wave are consistent with the drill-hole estimates of about 0.65 m for the ice thickness .

References

Sangfelt, E., Ivansson, S., and Karasalo, I, 2013. Under-ice shallow-water sound propagation and communication in the Baltic Sea. Proc. Meetings Acoustics (POMA), 19, 070044.

Ivansson, S., Karasalo, I, and Sangfelt, E., 2014. Three-dimensional ray modelling of high-frequency under-ice shallow-water sound propagation. Proc. 2nd International Conference and Exhibition on Underwater Acoustics, Rhodes, Greece, 963 – 970.

Dosso, S., Heard, G. J., and Vinnins, M., 2002. Source bearing estimation in the Arctic using ice-mounted geophones. J. Acoust. Soc. Am., 112, 2721 – 2734.

Aki, K., and Richards, P. G., 2002. Quantitative Seismology. Univ. Science Books.

Ewing, W. M., Jardetzky, W. S., and Press, F., 1957. Elastic Waves in Layered Media. Mc-Graw Hill.

Ivansson, S., 1998. RPRESS, oalib version, computer programs for seismo-acoustic wave-fileds in range-independent fluid-solid media. Available at http://oalib.hlsresearch.com (Last viewed 11 March 2015).

Ivansson, S., 1993. Delta-matrix factorization for fast propagation through solid layers in a fluid-solid medium. J. Comput. Phys., 108, 357 – 367.

Ivansson, S., 1997. The compound matrix method for multi-point boundary-value. Z. angew. Math. Mech., 77, 767 – 776.

Ivansson, S., and Karasalo, I., 1992. A high-order adaptive integration method for wave propagation in range-independent fluid-solid media. J. Acoust. Soc. Am., 92, 1569 – 1577.

Ivansson, S., 1998. A class of low-frequency modes in laterally homogeneous fluid-solid media. SIAM J. Appl. Math., 58, 1462 – 1508.

Stein, P. J., Euerle, S. E., and Parinella, J. C., 1998.Inversion of pack ice elastic wave data to obtain ice physical properties. J. Geophys. Res., 103(C10), 21783 – 21793.